Structure
Article

Structure and Functional Regulation of RipA, a Mycobacterial Enzyme Essential for Daughter Cell Separation

Alessia Ruggiero,[1] Daniela Marasco,[1,2] Flavia Squeglia,[1,2] Silvia Soldini,[3] Emilia Pedone,[1] Carlo Pedone,[2] and Rita Berisio[1,*]
[1]Institute of Biostructures and Bioimaging, CNR, Via Mezzocannone 16, I-80134, Naples, Italy
[2]Department of Biological Sciences-Biostructure Section, University of Naples "Federico II," I-80134, Naples, Italy
[3]Institute of Microbiology, Catholic University of the Sacred Heart, I-00168, Rome, Italy
*Correspondence: rita.berisio@unina.it
DOI 10.1016/j.str.2010.06.007

SUMMARY

Cell separation depends on cell-wall hydrolases that cleave the peptidoglycan layer connecting daughter cells. In *Mycobacterium tuberculosis*, this process is governed by the predicted endopeptidase RipA. In the absence of this enzyme, the bacterium is unable to divide and exhibits an abnormal phenotype. We here report the crystal structure of a relevant portion of RipA, containing its catalytic-domain and an extra-domain of hitherto unknown function. The structure clearly demonstrates that RipA is produced as a zymogen, which needs to be activated to achieve cell-division. Bacterial cell-wall degradation assays and proteolysis experiments strongly suggest that activation occurs via proteolytic processing of a fully solvent exposed loop identified in the crystal structure. Indeed, proteolytic cleavage at this loop produces an activated form, consisting of the sole catalytic domain. Our work provides the first evidence of self-inhibition in cell-disconnecting enzymes and opens a field for the design of novel antitubercular therapeutics.

INTRODUCTION

Bacterial cellular division ends with cell disconnection, a mechanism needed to disconnect the two new daughter sacculi after the cell division is completed, or at the very late step of cell division.

The process of daughter cell separation requires a delicate balance of cell wall hydrolases that cleave the septa connecting daughter cells. Cell-separating enzymes usually contain endopeptidase domains, like cysteine histidine amino peptidase (CHAP) or NLPC/P60 domains, and/or glucosaminidase domains (Layec et al., 2008, 2009; Rossi et al., 2009).

In the case of *Mycobacterium tuberculosis*, the causative agent of tuberculosis (Kaufmann, 2008; Warner and Mizrahi, 2007), both enzyme types are responsible for cell separation (Hett et al., 2007, 2008; Hett and Rubin, 2008). In particular, resuscitation promoting factors (RpfA-E), which are responsible for revival of *M. tuberculosis* from dormancy (Downing et al., 2005; Kana et al., 2008; Mukamolova et al., 1998, 2002), have been shown to be transglycosylases capable of hydrolyzing the glycosidic bonds of peptidoglycan chains (Ruggiero et al., 2009; Telkov et al., 2006). A key enzyme for *M. tuberculosis* cell division is resuscitation promoting factor interacting protein (RipA), which is believed to cleave peptidoglycan peptide crosslinks (Hett et al., 2008), similar to other cell separating endopeptidases, like CwlT from *Bacillus subtilis* (Fukushima et al., 2008) and Spr from *Escherichia coli* (Aramini et al., 2008). This enzyme colocalizes at bacterial septa with RpfB (Hett et al., 2007), the sole of the five Rpfs (A–E) encoded in *M. tuberculosis* genome to be not dispensable for bacterial revival in vivo (Tufariello et al., 2006). RipA has a remarkable effect on bacterial phenotype because *ripA* depletion strains in *Mycobacterium smegmatis* exhibit a decreasing growth and an abnormal phenotype, consisting in branching and chaining bacteria (Hett and Rubin, 2008). This makes RipA an excellent candidate as a drug target against tuberculosis.

The effect of cell wall hydrolases is two fold: (1) they alter mechanical properties of cell walls; and (2) they release soluble peptidoglycans that, as recently suggested, activate the serine/threonine kinase PknB (Kana and Mizrahi, 2010; Shah and Dworkin, 2010; Shah et al., 2008).

In a previous study, we have determined the crystal structure of a major portion of RpfB and suggested that the peculiarity of RpfB (Tufariello et al., 2006), compared to the other four members of the Rpf family, is its ability to anchor to the cell wall using the G5 domain (Ruggiero et al., 2009).

In this study, we investigate RipA function both biochemically and structurally, by combining atomic resolution X-ray crystallography, circular dichroism (CD) and fluorescence spectroscopy, and mass spectrometry. Besides an atomic resolution picture of RipA, this study yields new insights in the functional regulation of this enzyme. Indeed, the crystal structure clearly reveals a zymogenic nature of RipA, a finding that is confirmed by cell wall degradation assays. Redundancy in regulation mechanisms is of fundamental importance for this essential cell wall hydrolase that, if not regulated, is potentially suicidal.

Table 1. Data Collection and Refinement Statistics

Data collection	
Space group	$P2_12_12_1$
Unit-cell parameters *a*,*b*,*c* (Å)	36.77, 65.41, 67.79
Resolution shell (Å)	30.0–1.0
Unique reflections (n)	85,882
Average redundancy	12.2 (3.1)
R_{merge} (%)	8.0 (29.2)
Completeness (%)	96.5 (72.6)
Mean I/σ (I)	19.7 (3.0)
Refinement	
Resolution range (Å)	15.0–1.0
Rwork (%)	10.7
Rfree (%)	13.7
Atoms (n)	
Protein	1552
Water	390
Average atomic displacement parameters (Å^2)	
Protein main chain, side chain	9.8, 13.8
Water	28.3
Root mean square deviations	
Bond lengths (Å)	0.019
Bond angle distance (Å)	0.030
Mean coordinate error (Å)	0.021

Values in parentheses are for the highest resolution shell (1.04–1.00 Å). See also Figure S1.

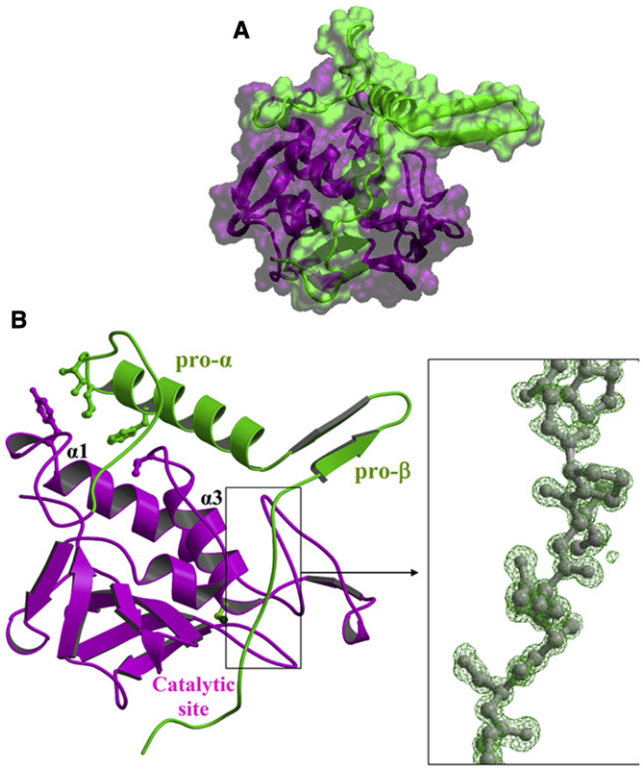

Figure 1. The Crystal Structure of $RipA_{263–472}$ Shows Self-Inactivation

(A) Solvent accessible surface of $RipA_{263–472}$. The figure shows the blockage of the catalytic domain (magenta) active site cleft by the PB15164 domain (green).

(B) Ribbon representation of $RipA_{263–472}$ and, in the right box, (2Fo-Fc) electron density map at the catalytic site locking loop of the PB15164 domain. See also Figures S1 and S2.

RESULTS AND DISCUSSION

The Atomic Resolution Structure of $RipA_{263–472}$ Reveals a Zymogenic Nature for RipA

In RipA sequence, four distinct regions can be identified: a signal peptide at its N terminus, two domains of unknown function denoted in PFAM-B as PB07342 and PB015164, which are mainly distributed in mycobacteria, and a predicted catalytic domain of the NlpC/P60 family at its C-terminus. Based on sequence analysis, we have cloned and expressed three RipA variants including: RipA deprived of its signal peptide ($RipA_{40–472}$), a shorter variant containing both the PB015164 and the catalytic domains ($RipA_{263–472}$), and the sole C-terminal catalytic domain ($RipA_{332–472}$). All recombinant proteins were found to be monomeric in solution, as evidenced by both size exclusion chromatography and light scattering (data not shown).

Crystals suitable for X-ray studies were obtained for $RipA_{263–472}$. The structure of $RipA_{263–472}$ was solved using the multiple anomalous dispersion (MAD) method and refined at atomic resolution (1.0 Å). For details of data processing, refinement, and structure validation see Table 1 and Figure S1 (available online).

The overall crystal structure shows that its two domains, the catalytic NlpC/P60 domain and the PB015164 domains identified in the PFAM database, are tightly bound (Figure 1). Surprisingly, we found that the catalytic site cleft of the enzyme is physically blocked by the PB015164 domain. This finding strongly suggests functional inactivity of the enzyme in this form and reveals a zymogenic nature for RipA.

The structure of RipA catalytic domain comprises a central β sheet of six antiparallel β strands, a small two-stranded β sheet and six helices, arranged in a αββααββββββ topology (Figure 2). Its putative catalytic cysteine (Cys383) is located at the N-terminal end of a helix (α2) and is packed against the six-stranded β sheet core (Figure 2). At this location, Cys383 facets another conserved residue, His432, belonging to the β strand β3 (Figure 2). This histidine is hydrogen bonded to the side chain of Glu444, which is in turn tightly anchored to Arg453 and Arg458 (Figure 2). Notably, the crystal structure shows that RipA contains a Cys-His-Glu catalytic triad, which is unusual in NlpC/P60 domains (Figure 3). A similar triad (Cys-His-Asp) characterizes another class of cysteine proteases involved in cell separation, denoted as CHAP domain containing proteases (Bateman and Rawlings, 2003; Rossi et al., 2009). As mentioned above, the crystal structure shows that RipA catalytic residues are not accessible to potential substrates (Figure 1), as they are locked by the PB015164 domain, here denominated prodomain. This domain, hitherto of unknown structure and function, contains a catalytic-cleft-blocking loop region, a β hairpin, and a long α helix, which is nearly perpendicular to the β hairpin

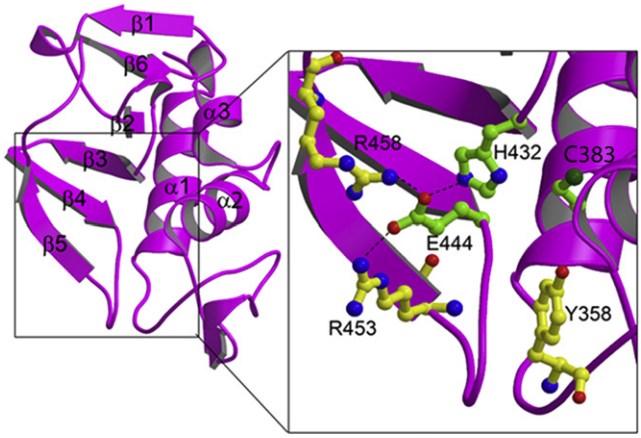

Figure 2. Topology of RipA Catalytic Domain and Zoom of the Catalytic Site

(Figures 1 and 4). A tight interaction between the catalytic domain and the prodomain is observed, with a total interaction surface area of 1809 Å^2. Whereas the β hairpin is nearly completely solvent exposed (Figure 1), both the catalytic-cleft-blocking loop region and the α helix, hereafter denoted as pro-α, establish several interactions with the main core of the RipA mature enzyme (Figure 1). Pro-α is an amphipathic helix, which is well anchored to the mature protein by hydrophobic and hydrogen bonding interactions. Its hydrophobic face packs against the N-terminal part of the α1-helix and the C-terminal part of the α3-helix (Figure 1). Furthermore, hydrogen bonds exist between the mature enzyme and the activation loop (e.g., between T232 and V394).

A strong contribution to interdomain interactions is also given by the catalytic-cleft blocking loop encompassing residues 263–283, with a total interaction surface of 899 Å^2 (~50% of the interdomain surface area). This loop displays a well-defined electron density, consistent with its tight binding to the catalytic cleft by several hydrogen bonds (Figure 1). These are main-chain main-chain hydrogen bonds, between S276 and S330, I279 and H300, main-chain side-chain hydrogen bonds between D268 and Q331, P272 and Q331, S276 and S430, and side-chain side-chain hydrogen bonds between D268 and R458, S276 and S402.

Besides providing the first structural description of the prodomain, our results elucidate its functional role. Using CD spectroscopy, we observed that the recombinant RipA$_{332–472}$, lacking the prodomain, is still able to fold (Figure S2). This finding suggests

```
RipA    PAGSAQGRIPRVYGRQASEYVIRRGMSQIGV-PYSWGGGNAAGPSKGIDSGAGTVGFDCSGLVLYSFAGV-GIKL----PHYSGSQYNL--GRKIPSSQMRRGDVIFYG-----PNGSQH
Q57223  ------------------------------------GVSRRG-------------VDCSGFVQKTFFDRFNLRL----PRSTVEQANY--GKHVRKEDIQTGDLIFFKTGR--GPNGYH
P45296  ------------------------------------GTTKRG-------------IDCSAFMQTTFSEVFGIEL----PRSTAEQRHL--GRKINKSELKKGDLVFFRK-------NNH
P0AFV6  ------------------------------------GSTKKG-------------IDCSGFVQRTFREQFGLEL----PRSTYEQQEM--GKSVSRSNLRTGDLVLFRA----GSTGRH
O35010  --------VPVSQQKGTAEDIIQTGAFFLGL-PYLWGGISGFG-------------FDCSGFMYSIFKAN-GYSI----PRDAGDQAKA--GKVVPLDDMKAGDLLFFAYEEG-KGAIHH
P76190  AASGTLADAHKAKVQKATKVAMNKLMQQIGK-PYRWGGSSPRT------------GFDCSGLVYYAYKDLVKIRI----PRTANEMYHLRDAAPIERSELKNGDLVFFRTQG--RGTADH
Q47151  -----------------TEVAIHRLEQQLGK-PYVWGGTRPDK------------GFDCSGLVFYAYNKILEAKL----PRTANEMYHYRRATIVANNDLRRGDLLFFHIHS--REIADH
Q65NQ9  ----------------AIEAAISTGSSIVGRSPYKWGGGRSQA-------DIDNRRFDCSSFVRWAYASA-GVELGF--GATTSTLVGK--GRAVSASEMKRGDLVFFDT----YKTNGH
P40767  ------------------EGAISVGSSIVGQSPYKFGGGRTQS-------DINNRIFDCSSFVRWAYASA-GVNLGPVGGTTTDTLVGR--GQAVSASEMKRGDLVFFDT----YKTNGH
P67473  --------------------VVQAALTQVGA-PYAWGGAAPGG-------------FDCSGLVMWAFQQA-GIAL----PHSSQALAHG--GQPVALSDLQPGDVLTF------YSDASH
P13692  --------------------IVAEAYKYIGT-PYVWGGKDPSG-------------FDCSGFTRYVYLQVTGRDI----GGWTVPQESA--GTKISVSQAKAGDLLFWGS----AGGTYH
P96740  --------------------VVQEAEKYIGV-PYVFGGSTPSE------------GFDCSGLVQYVFQQALGIYL----PRSAEQQWAV--GEKVAPQNIKPGDVVYFSNTY--KTGISH
O07532  --------------------MISAAKAQLGV-PYRWGGTTPSG-------------FDCSGFIYYVLNKV-T-SV----SRLTAAGYWN--TMK-SVSQPAVGDFVFFSTY---KAGPSH
O31852  PTKPKDNSGSNIQIGSKIDRMITEAKKYVGV-PYRWGGNTPAG-------------FDCSGFIYYLINNV-S-SI----SRLSTAGYWN--VMQ-KVSQPSVGDFVFFTTY---KSGPSH
P96645  ------------------ETVMKEALKYEGQ-PYAWGGSNPET------------GFDCSGLVQWSFAKA-GITL----PRTAQEQHGA--TKKISEKEATAGDLVFFGGTYE-GKAITH
Q01835  --------------------------HLGK-PYTWGARGPST-------------FDCSGFTSYVFNQV-GLSL----SGNSATQYAN--STKISESQAQPGDLVFFNY----GSGIAH
Q01838  --------------------IIAEAQKHLGK-AYSWGGNGPTT-------------FDCSGFTSYVFAQS-GITL----PRTSGAQYAS--TTKVSESEAQPGDLVFFDY----GSGIAH
Q01837  -------------------LIAEAQKHLGK-AYSWGGNGPTT-------------FDCSGFTKYVFAKS-GVTL----PRTSGAQYAS--STKISESQAKPGDLVFFDY----GNGIAH
Q01839  --------------------------HLGK-AYSWGGNGPTT-------------FDCSGFTSYVFAKS-GISL----PRTSGAQYAS--TSRISESQAKPGDLVFFDY----GSGIAH
P21171  --------------------IIAEAQKHLGK-AYSWGGNGPTT-------------FDCSGYTKYVFAKA-GISL----PRTSGAQYAS--TTRISESQAKPGDLVFFDY----GSGISH
Q01836  ---------------SASALIAEAQKHLGK-AYSWGGNGPTT-------------FDCSGFTKYVFAKS-GISL----PRTSGAQYAS--TTRISESQAKPGDLVFFDY----GSGISH
```

```
RipA            VTIYLGNGQMLEAPDVGLKVRVAPVRTAGMTPYVVRYIEY
Q57223          VGIYVKEDKFLHASTRG----------------------
P45296          VGVYIGNNQFMHA------------------------
P0AFV6          VGIYIGNNQFVHA------------------------
O35010          VGLYVGGGKMLHSPKTGKSIEI----------------
P76190          VGVYVGNGKFIQSPRTGQEIQI----------------
Q47151          MGVYLGDGQFIESPRTGETIRIS----------------
Q65NQ9          VGIYLGNGTFLN--------------------------
P40767          VGIYLGNGTFLN--------------------------
P67473          AGIYIGDGLMVHSSTYGVPVRVVPMDSSGPIYDARRY---
P13692          VAISLGGGQYIHAPQPGENVKVGSVQ------------
P96740          AGIYAGAGRFIQA------------------------
O07532          VGIYLGNGEFINANDSGVVI------------------
O31852          MGIYLGGGDFIHASSSGVDI------------------
P96645          VGIYVGNGRMFNSNDSGIQ-------------------
Q01835          VGIYIGGGQMIDAQDNGVSI------------------
Q01838          VGIYVGNGQMINAQDNGVK------------------
Q01837          VGIYVGNGQMINAQDNGVK------------------
Q01839          VGIYVGNGQMINAQDNGVK------------------
P21171          VGIYVGNGQMINAQDNGVK------------------
Q01836          VGIYVGNGQMINAQDNGVK------------------
```

Figure 3. Multiple Sequence Alignment of NlpC/P60 Domains Identified by CONSURF
Conserved Cys and His are highlighted in dark grey, the third catalytic residue is shown in light grey.

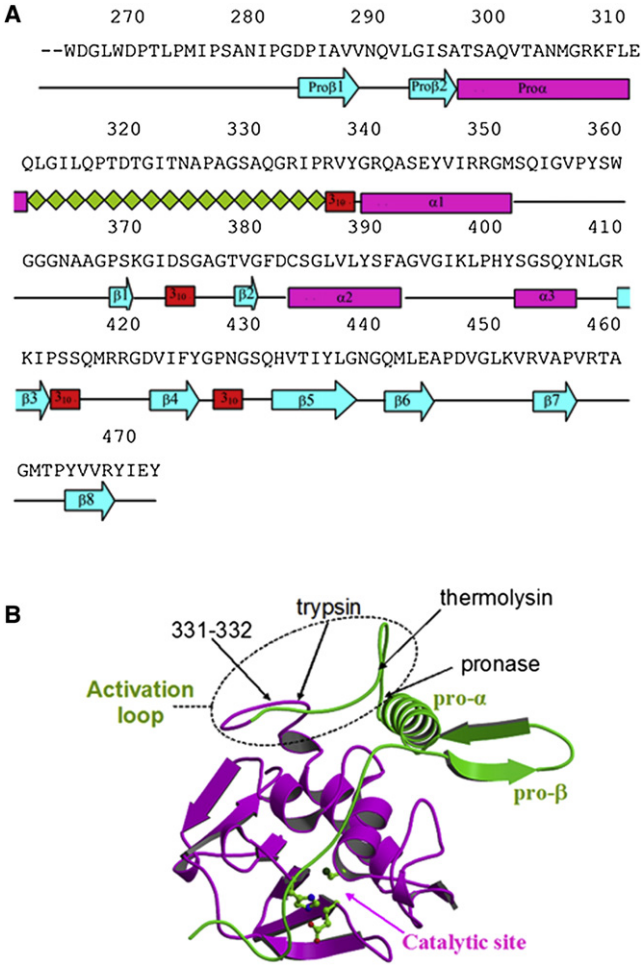

Figure 4. Location of Proteolytic Cleavage Sites

(A) Amino acid sequence and secondary structure elements of $RipA_{263–472}$.

(B) Ribbon structure of $RipA_{263–472}$ with proteolytic cleavage sites highlighted.

that the prodomain is not needed for enzyme folding, as observed for proteases of the cathepsin family (Menard et al., 1998). Instead, the X-ray structure reported here highlights a role of the prodomain as a regulator of the enzyme catalytic activity. With this concept in mind, we explored the possible mechanism that activates the zymogenic form of RipA and unlocks the catalytic site. A suggestion comes from the X-ray structure, which displays a peculiarly long and fully solvent exposed loop connecting the catalytic- and the prodomains (Figure 4). Furthermore, we observed that on storage, all recombinant RipA forms we produced were degraded to smaller fragments, with molecular weights (MW) close to 15 kDa. This MW, also checked by mass spectrometry, corresponded to the catalytic domain (residues 332–472, see Figures S3 and S4).

Limited Proteolysis Experiments

To investigate RipA vulnerability to proteases, we carried out limited proteolysis experiments by trypsin, thermolysin, and pronase (Figure 5). Using protease/enzyme concentration ratios of 1:500, these proteases were able to degrade $RipA_{263–472}$ to fragments of about 15 kDa (Figure 5). Cleavage sites by these proteases were identified using LC-MS analysis. As shown in Figure 4, all cleavage sites are located in the large and fully solvent exposed loop, which connects the catalytic NlpC/P60 domain and the prodomain. This shows that the connecting loop is a vulnerability point for the enzyme, as it is highly sensitive to proteolytic degradation. In addition, LC-MS analysis shows that, after proteolysis at the connecting loop (Figure 4), the prodomain is released and further proteolyzed.

Release of the Prodomain Activates RipA

Cell wall degrading experiments were carried out using lyophilized cells of *Micrococcus lysodeikticus* (ATCC No. 4698) labeled with fluorescein isothiocyanate (FITC) (see Experimental Procedures). Both recombinant $RipA_{263–472}$ and $RipA_{332–472}$ were incubated with the FITC-labeled cells. Peptidoglycan hydrolyzing activity of RipA forms was evaluated by fluorescence spectroscopy as the amount of FITC-labeled cell wall released in solution (Figure 6). Fluorescence measurements of supernatants at time intervals allowed us to characterize the time course of cell degrading reaction (Figure 6). The most evident result is that $RipA_{332–472}$ is able to degrade FITC-labeled cell wall because early incubation time intervals and its kinetics reaches a plateau after ~20 hr (Figure 6). By contrast, $RipA_{263–472}$ displayed hardly any activity after 20 hr (Figure 6). The digestion mixture deriving from the reaction of $RipA_{332–472}$ with FITC-conjugated cell walls was also analyzed by reverse phase liquid chromatography (RP-HPLC). The mass-analysis of RP-HPLC profile, followed at 434 nm (absorption maximum of FITC), evidenced the presence of several peptide fragments (Figure S5) labeled with a FITC moiety, with molecular weights ranging from 900 to 1300 Da. The chromatogram shows a main peak (~17 min) containing species with molecular weight close to 1100 Da (Figure S3). The same analysis, conducted on supernatants in the absence of the enzyme, evidenced no detectable cell wall fragments; this confirmed that the release of FITC labeled fragments in solution was due to RipA enzymatic action.

To investigate the role of the putative catalytic Cys383 in catalysis, we produced a mutant of $RipA_{332–472}$, where C383 was mutated to alanine. Using this mutant in the cell degrading experiments, we observed that its hydrolytic activity was completely suppressed (Figure 6). The same suppression of RipA activity was observed on treatment of the enzyme with the sulfhydryl-alkylating reagent iodoacetamide (data not shown). These results experimentally prove that RipA is a cysteine protease, as they demonstrate the fundamental role of Cys383 in catalysis. Furthermore, they confirm the result we derived from the X-ray structure that RipA exists as an inactive zymogen, and that removal of the prodomain activates the enzyme (Figures 1 and 4).

Because we observed some level of instability to proteolytic degradation of RipA variants produced, in particular on storage (Figure S3; Figure 6), we checked whether enzyme processing is an autocatalytic event, as observed for the lysosomal cysteine proteases cathepsins (Menard et al., 1998; Rozman et al., 1999; Wittlin et al., 1999). To this aim, we carried out a typical assay for the assessment of self-processing (Rozman et al., 1999), where the inactive mutant $RipA_{263–472}$ (C383A) was incubated with the activated $Rip_{332–472}$ form at room temperature. After 16 hr,

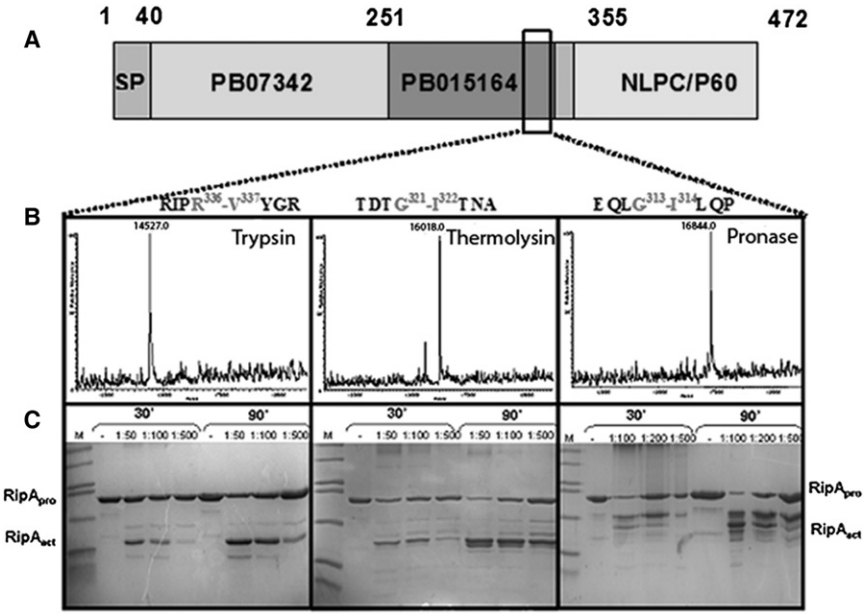

Figure 5. Limited Proteolysis Studies

(A) Schematic representation of RipA domains, as defined by PFAM. The region that was found to be sensitive to degradation is indicated by a black box. (B) Mass spectra of main RP-HPLC peaks after limited proteolysis of $RipA_{263–472}$ with trypsin, themolysin, and pronase. Cleavage sites are indicated. (C) Coomassie stained SDS-PAGE after limited proteolysis of $RipA_{263–472}$ with trypsin, themolysin, and pronase. Molecular mass markers from the top to bottom: 45, 36, 29, 24, 20, 14.2, 6.5 kDa. See also Figures S3 and S4.

SDS-PAGE analysis showed that $RipA_{332–472}$ is unable to process $RipA_{263–472}$ (C383A) (Figure 7). This result unambiguously showed that RipA is not self-activated, but it needs an activating mechanism. Thus far, it is unclear which mechanism is able to activate RipA. The strong susceptibility of the loop connecting the catalytic and prodomains to proteolytic degradation, as well as the tight interdomain interactions observed in the X-ray structure (Figure 1A) strongly suggests that activation proceeds via proteolytic cleavage. However, because RipA is able to interact with RpfB (Hett et al., 2008), we cannot exclude a possible alternative activation mechanism during resuscitation from latency, which involves a conformational change of RipA on RpfB binding and a consequent unlock of RipA catalytic site. It should be noted, however, that RipA has a fundamental role in cell disconnection of actively growing bacteria. The collective dispensability of all five Rpfs in in vitro bacterial growth (Kana et al., 2008) makes an activation mechanism via proteolytic processing more plausible, at least during bacterial active growth. Consistent with this observation, activation via proteolytic maturation is the typical activation mechanism of cysteine proteases (Schroder and Tschopp, 2010; Sripa et al., 2010).

In conclusion, our results provide a step forward in the molecular knowledge of the structural and functional properties of RipA in the peptidoglycan degradation process. We demonstrate that this enzyme, vital to *M. tuberculosis*, exists in a zymogenic form that needs to be activated. This evidences a regulation mechanism that is likely precious for a fundamental process like daughter cells separation. Finally, RipA is a secreted enzyme and easily accessible to drugs. Therefore, our study opens a field for the design of novel classes of antitubercular therapeutics.

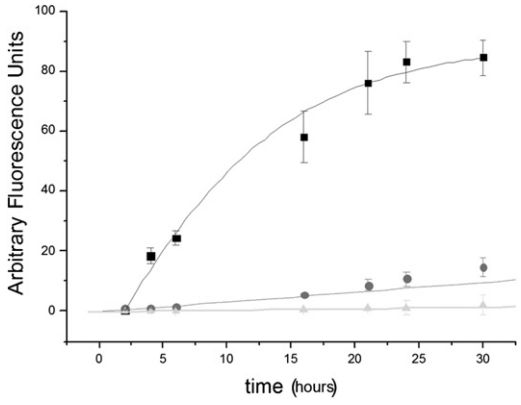

Figure 6. Cell Wall Degrading Activity of $RipA_{263–472}$, $RipA_{332–472}$ C383A Mutant, and $RipA_{332–472}$

$RipA_{263–472}$, $RipA_{332–472}$ C383A mutant, and $RipA_{332–472}$ shown as grey circles, light grey triangles, and black squares, respectively. Values were measured as the amount of FITC-labeled cell wall released in solution on incubation with the enzymes. The residual activity measured for $RipA_{263–472}$ at 30 hr was correlated, by LC-MS analysis, to the formation of small amounts of proteolytically processed enzyme.

EXPERIMENTAL PROCEDURES

Cloning, Expression, and Purification

RipA variants $RipA_{40–472}$ and $RipA_{263–472}$ and $RipA_{332–472}$ were designed based on the protein secondary structure predictions and protein domain organization, by consulting the PFAM database. $RipA_{263–472}$ was cloned, expressed and purified as described (Ruggiero et al., 2010). For the preparation of $RipA_{40–472}$ and $RipA_{332–472}$., PCR reactions were carried out to amplify the encoding sequences using the *M. tuberculosis* strain *H37Rv* as a template and forward oligonucleotides starting at the aspartic residue 40 and the glycine 332, respectively. NcoI/HindIII-digested fragments were cloned into the pETM-11 and pETM-20 vectors for $RipA_{40–472}$ and $RipA_{332–472}$., respectively. $RipA_{40–472}$ was expressed and purified with the same procedure described for $RipA_{263–472}$ (Ruggiero et al., 2010). Differently, $RipA_{332–472}$ was expressed as an N-terminal fusion protein in *E. coli* BL21Star(DE3) and purified by two consecutive Ni^{2+} affinity chromatographies and a gel filtration (Superdex 75 16/60). The protein was concentrated in Vivaspin concentrators, cutoff 5 kDa, and stored in 50 mM Tris/HCl, 150 mM NaCl, 5% (v/v) glycerol, pH 8.

Mutant Preparation

The plasmid expression vectors encoding the C383A mutation were generated by site-directed mutagenesis of wild-type plasmids pETM-30-$RipA_{263–472}$ and pETM-20-$RipA_{332–472}$ using the Stratagene QuikChange kit and the mutagenic primers 5′-CCGTCGGCTTCGACGCCTCAGGCCTGGTGTTG-3′ and 5′-CAAC ACCAGGCCTGAGGCGTCGAAGCCGACGG-3′. DNA sequencing confirmed

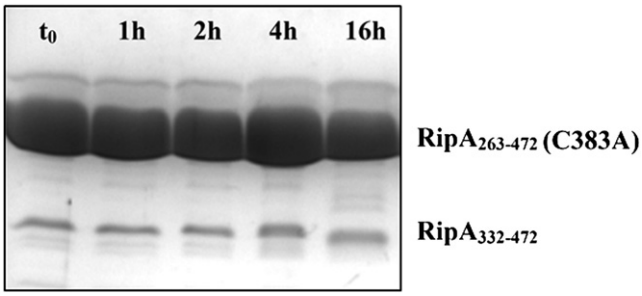

Figure 7. Coomassie stained SDS-PAGE after incubation of $RipA_{263–472}$ C383A mutant with $RipA_{332–472}$
Note that molar ratio is 20:1, in 20 mM Tris/HCl, pH 8. Incubation time is reported for each lane.

the mutations into the recombinant plasmid sequence. Expression and purification of the C383 ARipA mutants were carried out in the same conditions as for their unmutated enzymes.

Limited Proteolysis Experiments

$RipA_{263–472}$ was incubated at room temperature with trypsin, thermolysin, and pronase at various protease/enzyme ratios (1:50, 1:100, 1:200, and 1:500) in a suitable buffer containing 50 mM Tris/HCl pH 8 and 10 mM $CaCl_2$. Samples were taken after 30 and 90 min and the reactions stopped by adding SDS-PAGE sample buffer. The reaction products were analyzed by SDS-PAGE. Samples were also analyzed by mass spectrometry, after trypsin (1:50 ratio), thermolysin (1:100 ratio), and pronase (1:500 ratio) digestion.

Mass Spectrometry Studies

MS analysis was carried out on an LCQ DECA XP Ion Trap mass spectrometer (ThermoElectron, Milan, Italy) equipped with an OPTON ESI source (operating at 4.2-kV needle voltage and 320°C), and with a complete Surveyor HPLC system. Narrow bore 50 × 2 mm C18 BioBasic LC-MS columns from ThermoElectron were used for the analyses. LC binary gradient was from 5% to 70% of B (where B was CH_3CN 0.05% TFA, and A H_2O 0.08% TFA) in 45 min. Initial protein concentration was 22 μM (0.5 mg/mL). Three microliters of this solution were injected for all analyses. Mass spectra were recorded continuously between the mass range 400–2000 Da in positive mode. Multicharge spectra were deconvoluted using the BioMass program implemented in the Bioworks 3.1 package provided by the manufacturer.

CD

All CD spectra were recorded with a Jasco J-810 spectropolarimeter equipped with a Peltier temperature control system (Model PTC-423-S). Molar ellipticity per mean residue, $[\theta]$ in deg $cm^2 \times dmol^{-1}$, was calculated from the equation: $[\theta] = [\theta]_{obs} \times mrw \times (10 \times l \times C)^{-1}$, where $[\theta]_{obs}$ is the ellipticity measured in degrees, mrw is the mean residue molecular mass (105.3 Da), C is the protein concentration in $g \times L^{-1}$, and l is the optical path length of the cell in cm. Far-UV measurements (183–250 nm) were carried out at 20°C using a 0.1 cm optical path length cell and a protein concentration of 0.2 mg × mL^{-1}.

Inactivation of Cys383 RipA with Iodoacetamide

The unique sulfhydryl group of the Cys383 residue of RipA was chemically modified through alkylation with iodoacetamide. The reaction mixture contained 100 nmol (~4 μg) of protein I and 0.8 μl of 250 mM iodoacetamide (Sigma) in 50 mM NH_4HCO_3 (pH 8.0). The reaction was carried out for 30 min in the dark and then quenched by adding 30 μl of 2-mercaptoethanol. The chemical modification was checked by mass spectrometry that gave as an increased mass, compatible with the chemical modification inserted, 58 Da.

Crystallization, Data Collection, and Processing

Crystallization trials were carried out at 293 K using the hanging-drop vapor-diffusion method. Best crystals were obtained using 5–10 mg mL^{-1} protein solution and 8% (v/v) 2-propanol, 16% (w/v) PEG4000 in 60 mM sodium citrate trihydrate buffer, pH 5.6 (Ruggiero et al., 2010).

MAD data on a cryo-cooled Se-Met derivative crystal (100 K) of $RipA_{263–472}$ were collected on beamline BM14 at the ESRF (Grenoble, France) at the three wavelengths determined from the selenium absorption spectrum. A native data set was also recorded at the BM14 beamline (Table 1). Cryoprotection of the crystals was achieved by a fast soaking in a solution containing glycerol to a final concentration of 30% (v/v). The data sets were scaled and merged using HKL2000 program package (Otwinowski and Minor, 1997). Statistics of data collection are reported in Table 1.

Structure Determination

The crystal structure of the enzyme was solved by MAD using the anomalous signal from the Se atoms of selenomethionine-labeled. The program SOLVE (Terwilliger, 2004) was used to localize the selenium sites present in the asymmetric unit and to derive the experimental phases. Phases were improved by density modification using the programs RESOLVE (Terwilliger, 2004) and wARP (Langer et al., 2008). Crystallographic refinement was first carried out against 95% of the measured data using the CCP4 program suite (Potterton et al., 2003). The remaining 5% of the observed data, which was randomly selected, was used in Rfree calculations to monitor the progress of refinement.

The refinement in Refmac was started using data up to 1.7 Å resolution and gradually increased in subsequent rounds of refinement to the highest resolutions (Murshudov et al., 1997). At this stage, water molecules were incorporated into the structure in several rounds of successive refinement. This refined model was used to carry out CGLS refinement using SHELXL97 (Sheldrick, 2008), where X-ray intensities were used in refinement calculations. The bond distances and angles (1,2 and 1,3 distances) were restrained using standard Engh and Huber restraints (Engh and Huber, 1991). Each round of refinement with SHELXL consisted of 10 cycles of restrained CGLS refinement followed by manual model adjustments using (2Fo − Fc) and (Fo − Fc) electron-density maps. Initial rounds of restrained CGLS refinement were carried out by keeping all atomic displacement parameters (ADPs) isotropic. Subsequently, the ADPs were converted to anisotropic values, leading to improved Fourier maps. At this stage, alternative conformations visible in the electron-density maps were modeled and refined isotropically before being refined anisotropically. The bulk solvent was modeled based on Babinet's principle, as implemented in the SWAT option in the SHELXL program. An approximate isotropic behavior was attributed to solvent atoms (ISOR restraint). The final round of refinement was carried out with the inclusion of riding H atoms for protein residues. The positions of H atoms assigned based on the known geometrical criteria were not refined. A blocked matrix least-squares minimization was carried out to estimate individual parameter uncertainties. Their mean value, as estimated after the inversion of the least square matrix, is reported in Table 1. The protein molecule was split into five overlapping blocks, with five residues of overlap and approximately equal numbers of parameters. Refinement of the positional parameters of solvent molecules was carried out in a single block. Structures were validated using the program PROCHECK (Laskowski et al., 1996).

Cell Wall Degradation Assays

Inactivated lyophilized cells of *M. lysodeikticus* (ATCC No. 4698) were labeled with FITC by covalently linking FITC to amine groups in the cell wall. In this reaction, 40 mg cells were incubated at 20°C with 20 mg FITC (50 mg/mL) in 100 mM $NaCO_3$, pH 8.5, protected from light. After 16 hr incubation, the reaction mixture was centrifuged; the insoluble material was washed until the supernatant was completely colorless, to eliminate unreacted fluorochrome. The labeled insoluble material was re-suspended and stored at −20°C in a 4× reaction buffer (50 mM Tris-HCl, 10 mM $MgCl_2$, 2 mM $MnCl_2$, 100 mM NaH_2PO_4, 50 mM KCl, 0.01% (v/v) CHAPS). $RipA_{263–472}$, $RipA_{332–472}$ (C383A), and $RipA_{332–472}$ were incubated with FITC-labeled cells at 30°C in the reaction buffer; the insoluble substrate was centrifuged (16,000 × g) and soluble FITC-conjugates were measured in triplicate with filters for excitation at 492 nm and emission at 518 nm. The buffer alone was used to correct for background release of FITC.

ACCESSION NUMBERS

Coordinates and structure factors have been deposited in the Protein Data Bank with accession number 3NE0.

SUPPLEMENTAL INFORMATION

Supplemental Information includes Supplemental Results and five figures and can be found with this article online at doi:10.1016/j.str.2010.06.007.

ACKNOWLEDGMENTS

This work has been funded by the MIUR (FIRB, contract RBRN07BMCT). We thank G. Delogu for fruitful discussion. We also acknowledge assistance from the ESRF staff (beamline BM14, Grenoble, France).

Received: April 27, 2010
Revised: June 9, 2010
Accepted: June 17, 2010
Published: September 7, 2010

REFERENCES

Aramini, J.M., Rossi, P., Huang, Y.J., Zhao, L., Jiang, M., Maglaqui, M., Xiao, R., Locke, J., Nair, R., Rost, B., et al. (2008). Solution NMR structure of the NlpC/P60 domain of lipoprotein Spr from Escherichia coli: structural evidence for a novel cysteine peptidase catalytic triad. Biochemistry *47*, 9715–9717.

Bateman, A., and Rawlings, N.D. (2003). The CHAP domain: a large family of amidases including GSP amidase and peptidoglycan hydrolases. Trends Biochem. Sci. *28*, 234–237.

Downing, K.J., Mischenko, V.V., Shleeva, M.O., Young, D.I., Young, M., Kaprelyants, A.S., Apt, A.S., and Mizrahi, V. (2005). Mutants of Mycobacterium tuberculosis lacking three of the five rpf-like genes are defective for growth in vivo and for resuscitation in vitro. Infect. Immun. *73*, 3038–3043.

Engh, R.A., and Huber, R. (1991). Accurate bond and angle parameters for X-ray protein structure refinement. Acta Crystallogr. A *47*, 392–400.

Fukushima, T., Kitajima, T., Yamaguchi, H., Ouyang, Q., Furuhata, K., Yamamoto, H., Shida, T., and Sekiguchi, J. (2008). Identification and characterization of novel cell wall hydrolase CwlT: a two-domain autolysin exhibiting n-acetylmuramidase and DL-endopeptidase activities. J. Biol. Chem. *283*, 11117–11125.

Hett, E.C., and Rubin, E.J. (2008). Bacterial growth and cell division: a mycobacterial perspective. Microbiol. Mol. Biol. Rev. *72*, 126–156.

Hett, E.C., Chao, M.C., Steyn, A.J., Fortune, S.M., Deng, L.L., and Rubin, E.J. (2007). A partner for the resuscitation-promoting factors of Mycobacterium tuberculosis. Mol. Microbiol. *66*, 658–668.

Hett, E.C., Chao, M.C., Deng, L.L., and Rubin, E.J. (2008). A mycobacterial enzyme essential for cell division synergizes with resuscitation-promoting factor. PLoS Pathog. *4*.

Kana, B.D., and Mizrahi, V. (2010). Resuscitation-promoting factors as lytic enzymes for bacterial growth and signaling. FEMS Immunol. Med. Microbiol. *58*, 39–50.

Kana, B.D., Gordhan, B.G., Downing, K.J., Sung, N., Vostroktunova, G., Machowski, E.E., Tsenova, L., Young, M., Kaprelyants, A., Kaplan, G., and Mizrahi, V. (2008). The resuscitation-promoting factors of Mycobacterium tuberculosis are required for virulence and resuscitation from dormancy but are collectively dispensable for growth in vitro. Mol. Microbiol. *67*, 672–684.

Kaufmann, S.H. (2008). Tuberculosis: Deadly combination. Nature *453*, 295–296.

Langer, G., Cohen, S.X., Lamzin, V.S., and Perrakis, A. (2008). Automated macromolecular model building for X-ray crystallography using ARP/wARP version 7. Nat. Protoc. *3*, 1171–1179.

Laskowski, R.A., Rullmannn, J.A., MacArthur, M.W., Kaptein, R., and Thornton, J.M. (1996). AQUA and PROCHECK-NMR: programs for checking the quality of protein structures solved by NMR. J. Biomol. NMR *8*, 477–486.

Layec, S., Decaris, B., and Leblond-Bourget, N. (2008). Diversity of Firmicutes peptidoglycan hydrolases and specificities of those involved in daughter cell separation. Res. Microbiol. *159*, 507–515.

Layec, S., Gerard, J., Legue, V., Chapot-Chartier, M.P., Courtin, P., Borges, F., Decaris, B., and Leblond-Bourget, N. (2009). The CHAP domain of Cse functions as an endopeptidase that acts at mature septa to promote Streptococcus thermophilus cell separation. Mol. Microbiol. *71*, 1205–1217.

Menard, R., Carmona, E., Takebe, S., Dufour, E., Plouffe, C., Mason, P., and Mort, J.S. (1998). Autocatalytic processing of recombinant human procathepsin L. Contribution of both intermolecular and unimolecular events in the processing of procathepsin L in vitro. J. Biol. Chem. *273*, 4478–4484.

Mukamolova, G.V., Kaprelyants, A.S., Young, D.I., Young, M., and Kell, D.B. (1998). A bacterial cytokine. Proc. Natl. Acad. Sci. USA *95*, 8916–8921.

Mukamolova, G.V., Turapov, O.A., Young, D.I., Kaprelyants, A.S., Kell, D.B., and Young, M. (2002). A family of autocrine growth factors in Mycobacterium tuberculosis. Mol. Microbiol. *46*, 623–635.

Murshudov, G.N., Vagin, A.A., and Dodson, E.J. (1997). Refinement of macromolecular structures by the maximum-likelihood method. Acta Crystallogr. D Biol. Crystallogr. *53*, 240–255.

Otwinowski, Z., and Minor, W. (1997). Processing of X-ray diffraction data collected in oscillation mode. Methods Enzymol. *276*, 307–326.

Potterton, E., Briggs, P., Turkenburg, M., and Dodson, E. (2003). A graphical user interface to the CCP4 program suite. Acta Crystallogr. D Biol. Crystallogr. *59*, 1131–1137.

Rossi, P., Aramini, J.M., Xiao, R., Chen, C.X., Nwosu, C., Owens, L.A., Maglaqui, M., Nair, R., Fischer, M., Acton, T.B., et al. (2009). Structural elucidation of the Cys-His-Glu-Asn proteolytic relay in the secreted CHAP domain enzyme from the human pathogen Staphylococcus saprophyticus. Proteins *74*, 515–519.

Rozman, J., Stojan, J., Kuhelj, R., Turk, V., and Turk, B. (1999). Autocatalytic processing of recombinant human procathepsin B is a bimolecular process. FEBS Lett. *459*, 358–362.

Ruggiero, A., Tizzano, B., Pedone, E., Pedone, C., Wilmanns, M., and Berisio, R. (2009). Crystal structure of the resuscitation-promoting factor $_{\Delta DUF}$RpfB from M. tuberculosis. J. Mol. Biol. *385*, 153–162.

Ruggiero, A., Squeglia, F., Esposito, C., Marasco, D., Pedone, E., Pedone, C., and Berisio, R. (2010). Expression, purification, crystallization and preliminary X-ray crystallographic analysis of the resuscitation promoting factor interacting protein RipA from M. tuberculosis. Protein Pept. Lett. *17*, 70–73.

Schroder, K., and Tschopp, J. (2010). The inflammasomes. Cell *140*, 821–832.

Shah, I.M., and Dworkin, J. (2010). Induction and regulation of a secreted peptidoglycan hydrolase by a membrane Ser/Thr kinase that detects muropeptides. Mol. Microbiol.

Shah, I.M., Laaberki, M.H., Popham, D.L., and Dworkin, J. (2008). A eukaryotic-like Ser/Thr kinase signals bacteria to exit dormancy in response to peptidoglycan fragments. Cell *135*, 486–496.

Sheldrick, G.M. (2008). A short history of SHELX. Acta Crystallogr. A *64*, 112–122.

Sripa, J., Laha, T., To, J., Brindley, P.J., Sripa, B., Kaewkes, S., Dalton, J.P., and Robinson, M.W. (2010). Secreted cysteine proteases of the carcinogenic liver fluke, Opisthorchis viverrini: regulation of cathepsin F activation by autocatalysis and trans-processing by cathepsin B. Cell Microbiol. *12*, 781–795.

Telkov, M.V., Demina, G.R., Voloshin, S.A., Salina, E.G., Dudik, T.V., Stekhanova, T.N., Mukamolova, G.V., Kazaryan, K.A., Goncharenko, A.V., Young, M., and Kaprelyants, A.S. (2006). Proteins of the Rpf (resuscitation promoting factor) family are peptidoglycan hydrolases. Biochemistry (Mosc.) *71*, 414–422.

Terwilliger, T. (2004). SOLVE and RESOLVE: automated structure solution, density modification and model building. J. Synchrotron Radiat. *11*, 49–52.

Tufariello, J.M., Mi, K., Xu, J., Manabe, Y.C., Kesavan, A.K., Drumm, J., Tanaka, K., Jacobs, W.R., Jr., and Chan, J. (2006). Deletion of the Mycobacterium tuberculosis resuscitation-promoting factor Rv1009 gene results in delayed reactivation from chronic tuberculosis. Infect. Immun. *74*, 2985–2995.

Warner, D.F., and Mizrahi, V. (2007). The survival kit of Mycobacterium tuberculosis. Nat. Med. *13*, 282–284.

Wittlin, S., Rosel, J., Hofmann, F., and Stover, D.R. (1999). Mechanisms and kinetics of procathepsin D activation. Eur. J. Biochem. *265*, 384–393.

